Int. J. Heat Mass Transfer. Vol. 26, No. 1, pp. 23–32, 1983
Printed in Great Britain

0017-9310/83/010023-10 $03.00/0

ENTRANCE REGION HEAT TRANSFER IN A UNIFORM WALL-TEMPERATURE HELICAL COIL WITH TRANSITION FROM TURBULENT TO LAMINAR FLOW

C. E. KALB
Air Products and Chemicals Inc., Box 538, Allentown, PA 18105, U.S.A.

and

J. D. SEADER
Department of Chemical Engineering, University of Utah,
Salt Lake City, UT 84112, U.S.A.

(*Received* 3 *June* 1981 *and in final form* 3 *May* 1982)

Abstract—Entrance-region heat transfer to gases flowing in a uniform wall-temperature helical coil was studied experimentally. A novel gradient method of heat transfer investigation was developed based on measurement of the wall internal and external surface-temperature distributions. Runs were made in the range of Reynolds numbers where the flow is initially turbulent upon entering the coil, but laminar downstream where secondary flow develops. No prior measurements of local heat transfer coefficients have been reported for this flow regime or thermal boundary condition. The results indicate a rapid transition to laminar flow and are in satisfactory agreement with a numerical solution for fully developed heat transfer.

NOMENCLATURE

a, internal radius of tube;
c_p, specific heat at constant pressure;
d, internal diameter of tube;
De, Dean number, $Re\,(a/R)^{1/2}$;
G, mass flow rate per unit cross-sectional area;
h, local heat transfer coefficient, $q/(\bar{T}_w - T_b)$;
$\bar{h}$, peripherally averaged heat transfer coefficient, $\bar{q}/(\bar{T}_w - T_b)$;
k, thermal conductivity of fluid;
k_w, thermal conductivity of wall;
L, length of coil;
Nu, local Nusselt number, $2ha/k$;
$\overline{Nu}$, peripherally averaged Nusselt number, $2\bar{h}a/k$;
Nu_{lm}, average Nusselt number based on logarithmic-mean temperature difference;
Pr, Prandtl number, $c_p\mu/k$;
q, local heat flux at inside surface of coil;
$\bar{q}$, peripherally averaged heat flux at a given axial position;
q_{avg}, heat flux averaged over the inside surface of the coil;
r, radial coordinate in the tube wall cross section;
R, distance perpendicular from coil axis to tube center line;
R/a, curvature-ratio parameter;
Re, Reynolds number, dG/μ;
T, temperature;
T_b, local bulk fluid temperature;
T_w, local wall temperature;
$\bar{T}_w$, peripherally averaged inside wall temperature at a given axial position;
x, distance along center line of tube in streamwise direction.

Greek symbols

θ, angular coordinate in the tube wall cross section;
μ, viscosity;
ξ, parameter in boundary layer model.

Subscripts

0–7, numbers denoting equally spaced axial positions on coil;
c, critical value for transition to turbulent flow;
in, at inlet of coil;
out, at outlet of coil;
s, straight tube;
∞, fully developed.

INTRODUCTION

HEAT transfer to fluids flowing in curved tubes and coils with a circular cross section is of interest in many applications. Compared with straight-tube flow, the induced secondary flow in curved tubes causes a higher streamwise pressure gradient, a higher critical Reynolds number for transition to turbulent flow, higher average heat and mass transfer coefficients, and significant peripheral variation of transfer coefficients. Fully developed laminar curved-tube flow is characterized primarily by the Dean number, $De = Re\,(a/R)^{1/2}$. For $R/a \lesssim 10$, there is a slight additional dependence

on the bend-to-tube radius ratio (R/a), above that expressed in the Dean number. For helical coils, the coil pitch enters as another parameter, but Manlapaz and Churchill [1] have shown that this effect is significant only when the pitch is greater than the coil radius R. White [2] deduced from friction-factor measurements in coils that the critical Reynolds number increases as R/a is decreased. Taylor [3] verified this with dye-injection experiments and observed that, when the coil Reynolds number was between the straight-tube and curved-tube critical values, a laminar secondary flow pattern was established downstream, even though the flow was highly turbulent upon entering the coil. For a coil with $R/a = 18.7$, the transition from an initially turbulent straight-tube profile to laminar curved-tube flow occurred somewhere within the first turn of the coil for $2020 \leqslant Re \leqslant 5830$.

Recent studies [4–9] show that, compared with straight tubes, the hydrodynamic entrance length in curved tubes is relatively short. For developing curved-tube laminar flow with a parabolic velocity profile at the inlet, the experimental data of Austin and Seader [4], supported by the numerical computations of Patankar *et al.* [5], indicate that velocity profiles are essentially fully established within the first quarter-turn of a coil. Short curved-tube hydrodynamic entrance lengths are also found for turbulent flow [6].

For curved-tube laminar-flow heat transfer, numerical solution of the governing equations has provided the most useful results to date, and fully developed Nusselt numbers have been reported for the two boundary conditions of axially uniform wall heat flux with peripherally uniform wall temperature (UHF) [10–12] and axially and peripherally uniform wall temperature (UWT) [13–15]. The latter condition is also referred to as "constant wall temperature". Numerical solutions are also available for developing heat transfer with fully developed laminar flow [14, 16–18]. These latter numerical studies, supported by experimental work in electrically heated tubes [16, 18, 19], suggest that the thermal entrance region in curved tubes is also generally much shorter than that in straight tubes.

No curved-tube local heat transfer coefficient measurements of any kind have been reported for the UWT boundary condition. The present study was undertaken to devise a method for making such measurements. Local heat transfer coefficients, which varied both axially and peripherally, were measured for flow of gases (air and helium) in a two-turn helical coil with $R/a = 15.06$. Results were obtained for the regime where both turbulent and laminar flow exist simultaneously in different regions of the coil [3]. While important in practice, the effect on heat transfer of this turbulent–laminar transition has not been studied previously.

DESCRIPTION OF EXPERIMENTAL METHOD

The method devised for measuring local heat transfer coefficients under UWT conditions involved measurement of surface temperature distributions (peripheral and axial) at the inside and outside surfaces of a coil heated by a fluid condensing on the outside surface. Temperatures measured within the wall close to the inside and outside surfaces were extrapolated to give the surface temperatures. Numerical solution of Laplace's equation for steady conduction within the wall using the measured boundary conditions (the extrapolated surface temperature distributions) completely specified the thermal state of the wall. Local heat fluxes to the gas flowing inside the coil were determined from the numerically calculated local temperature gradients within the wall at the inside surface. Once the heat flux distribution was determined, the gas bulk temperature was calculated as a function of axial position and local heat transfer coefficients were defined. While the method requires that finite temperature drops of varying magnitude occur across the tube wall, in practice these temperature drops can be kept quite small, approximating closely the UWT boundary condition. In addition, the experimental conditions were such that axial temperature gradients within the wall were no greater than about 1% of the temperature gradients in either the radial or angular directions. Laplace's equation could therefore be treated locally as a 2-dim. problem in r and θ at each of the instrumented axial positions. Neglecting axial conduction, Laplace's equation in toroidal coordinates [11, 15] is

$$\frac{\partial^2 T_w}{\partial r^2} + \left(\frac{1}{r} + \frac{\sin\theta}{R + r\sin\theta}\right)\frac{\partial T_w}{\partial r} + \frac{1}{r^2}\frac{\partial^2 T_w}{\partial \theta^2} + \frac{\cos\theta}{r(R + r\sin\theta)}\frac{\partial T_w}{\partial \theta} = 0. \quad (1)$$

Equation (1) was solved numerically at each of six axial positions on the coil. Because of symmetry about the tube diameter parallel with the coil radius R, only half of the tube wall cross-section needed to be instrumented and included in the numerical solution. The interval $-\pi/2 \leqslant \theta \leqslant \pi/2$ was divided into 16 equal angular increments and the wall thickness was divided into 10 equal radial increments. Discretization of equation (1) using first-central difference operators resulted in a set of 153 linear equations for the unknown interior wall temperatures. These were solved by direct Crout reduction. Radial temperature gradients within the wall at the outside and inside surfaces were calculated using second-backward and second-forward difference operators, respectively. At each axial position, a heat balance at the outside and inside surfaces agreed to within 1% or less, indicating that numerical error was negligible.

Local heat fluxes to the gas were calculated from

$$q = k_w \left(\frac{\partial T_w}{\partial r}\right)_{r=a}. \quad (2)$$

Local and peripherally averaged Nusselt numbers were referred to the difference between the local peripherally averaged wall temperature at the inside surface and the local gas bulk temperature and are given, respectively, by

$$Nu = \frac{h2a}{k} = \frac{q2a}{k(\bar{T}_w - T_b)} \quad (3)$$

and

$$\overline{Nu} = \frac{\bar{h}2a}{k} = \frac{\bar{q}2a}{k(\bar{T}_w - T_b)} \quad (4)$$

where k is evaluated at the local gas bulk temperature. Air thermal conductivity and viscosity and k_w for type-304 stainless steel were obtained from ref. [20]. Thermal conductivity data for this steel from three independent studies were well correlated with a least-squares curve fit over the interval 200–600 K, and k_w was evaluated at the coil average wall temperature. This temperature was only slightly below that of the fluid condensing outside the coil, and a constant value of $k_w = 16.4\,\mathrm{W\,m^{-1}\,K^{-1}}$ (estimated accuracy ± 2%) resulted for all runs.

To be consistent with rigorous treatment using toroidal coordinates [11, 15], the peripherally averaged heat flux at a given axial position on the coil was evaluated numerically from

$$\bar{q} = \frac{1}{\pi(R/a)} \int_{-\pi/2}^{\pi/2} q(R/a + \sin\theta)\,d\theta. \quad (5)$$

A similar expression was used to evaluate $\bar{T}_w$ at each axial position.

Two-dimensional variations of the above method have been presented in the Russian literature for various axisymmetric straight-tube configurations and boundary conditions [21–26], where it is referred to as the "gradient method". However, application of the method to a 3-dim. problem and the close approximation to the UWT boundary condition treated here are believed to be unique.

Table 1. Dimensions and parameters of the helical coil

Number of turns	2
Radius of coil, R	16.00 cm
Average internal diameter*, d	2.125 cm
Average internal radius, a	1.0625 cm
Curvature ratio, R/a	15.06
Coil pitch	3.66 cm
Length of coil, L	201.2 cm
Dimensionless length, L/d	94.68
Average wall thickness	0.597 cm
Inside surface area	0.1343 m²
Cross sectional flow area	0.0003546 m²

*Determined gravimetrically by filling the coil with water.

EXPERIMENTAL APPARATUS AND PROCEDURES

The helical coil test section

The helical coil was fabricated commercially from seamless type-304 ss pipe. Stainless steel was chosen because its relatively low thermal conductivity results in measurable temperature drops across the wall of the coil. As received, the coil had four complete turns. A test section consisting of exactly two turns (4π rad) of uniformly curved pipe was cut from the original coil. Measurements of wall thickness and flow cross-section were made at the exposed cross-section. Only a slight ellipticity of the flow cross-section and distortion of wall thickness were introduced by the bending process. Two short straight lengths (2.2 cm) of the same pipe were threaded internally and soldered to the ends of the coil. Table 1 lists the dimensions and parameters of the finished coil.

Two nylon transition pieces 8.10 cm long were threaded into the ends of the coil to minimize end conduction losses. Two 89 cm lengths of carbon steel pipe with the same inside diameter as the coil were connected to the nylon transition pieces to provide a total straight length of 46 tube diameters at the coil inlet and exit. No discontinuities in the flow cross-section occurred in passing from one end of the final test assembly to the other. Five 200-mesh screens were placed at the beginning of the straight sections. Since all but one of the experimental runs [27] had entering Reynolds numbers greater than 2500, the screens ensured that turbulence was tripped in the straight section. For straight tubes, initially flat, turbulent velocity profiles become fully developed well within 46 diameters of the entrance [28]; therefore, fully developed, straight-tube, turbulent velocity profiles existed at the coil inlet for all but one of the runs.

Overall apparatus

Figure 1 is a schematic diagram of the overall

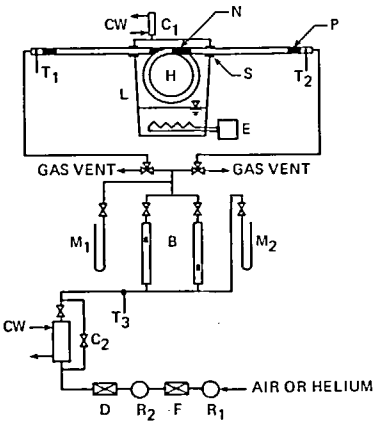

FIG. 1. Schematic diagram of the overall apparatus: B, rotameter bank; C_1, condenser; C_2, gas cooler; D, drier; E, electric heater and powerstat; F, filter; H, helical coil; L, tank containing 1,1,1-trichloroethane; M_{1-2}, mercury manometers; N, nylon transition piece; P, copper-mesh pad; R_{1-2}, primary and secondary regulators; S, nylon sleeve; T_{1-3}, glass thermometers.

apparatus. Gas was supplied from cylinders. A small water-cooled heat exchanger allowed close control of gas temperature and was used to cool the inlet gas to slightly below room temperature. Temperature drops across the wall of the coil were very small in some instances, especially at the lower flow rates and near the coil outlet. Cooling the inlet gas increased these temperature drops and improved the accuracy of the measurements.

The coil was suspended inside a tank containing 1,1,1-trichloroethane. Power input to the submerged electric heater was increased until condensate was observed in the condenser above the tank. A drip pan mounted above the coil prevented condensate from falling on the coil. The temperature of the saturated vapor surrounding the coil was about 69°C for all runs and was measured with a calibrated thermocouple.

Thirty copper–constantan thermocouples for measuring temperatures within the wall of the coil were installed on one of the two turns of the coil, and two three-way valves were provided so that the gas could be directed through the coil in either direction. This allowed the thermocouples to serve double duty, since thermocouples on the leading half of the coil became thermocouples on the last half of the coil if the flow direction was reversed. Therefore, a run was conducted in two steps, each with the gas flowing in the opposite direction through the coil. A total of 60 wall temperature measurements were made for each run.

Gas temperatures were measured with calibrated thermometers at the ends of the straight sections connected to the coil. Copper-mesh pads adjacent to the screens in the straight sections (on the side away from the coil) provided thermal mixing of the leaving gas. To obtain T_b directly at the coil inlet and outlet, heat losses or gains along the entire length of the straight sections were taken into account. Using a combination of guard heaters, measured temperature drops across insulation and analysis, corrections were made for heat transfer through the insulated straight sections of pipe outside the tank, the nylon sleeves in the walls of the tank, the insulated straight sections of pipe inside the tank, and the uninsulated nylon transition pieces. The latter correction was calculated iteratively using Nusselt's equation for condensation on a horizontal cylinder, coupled with equations for conduction through the nylon wall and convection inside the nylon pieces. The cumulative heat loss or gain corrections for the straight inlet or outlet sections were estimated to have a maximum uncertainty of $\pm 25\%$. This uncertainty affected the calculated values of $\overline{Nu}$ in the coil only by $\pm 4\%$.

Wall temperature measurements

The 30 copper–constantan wall temperature thermocouples were made from type-304 ss sheathed elements (1.03 mm O.D.). With the aid of a microscope and miniature torch, a very small bead junction was formed and centered at the tip of each thermocouple and then covered with epoxy cement. The thermocouples were calibrated in 1°C increments from 57°C to 75°C using a constant-temperature bath (± 0.01°C), NBS-certified thermometers (graduated to 0.1°C), and individual ice-bath reference junctions. Using the same data-logging system which would be used during the heat transfer tests, 10 printouts of the calibration data were obtained at each temperature; these were then averaged for each thermocouple. Calibration data for each thermocouple were correlated by least-squares polynomial fit, with a standard deviation of 0.01°C and a maximum deviation of 0.03°C. The thermoelectric power of these thermocouples at 70°C is $45\,\mu V°C^{-1}$. Since voltage was determined to $\pm 1\,\mu V$, the maximum attainable accuracy in the wall-temperature measurements was ± 0.02°C.

After calibration, the 30 thermocouples were mounted within the wall of the coil, with 10 thermocouples placed at each of three axial positions on the first turn of the coil. Three additional instrumented axial positions were effectively obtained by reversing the flow direction through the coil. The axial positions were chosen so that the coil's two turns were divided into seven sections of equal length. Therefore, the six axial positions were spaced at angular intervals of $4\pi/7$ rad along the coil (13.53 tube i.d.).

At each axial position, five pairs of thermocouples were spaced equally over the interval $-\pi/2 \leqslant \theta \leqslant \pi/2$, i.e., from the inner to the outer bends of the flow cross-section. Five of these thermocouples were placed in 1.09 mm holes drilled normal to the surface with the bottom of the holes close to the inside surface of the coil, and the other five were placed in shallow grooves (1.19 mm wide and deep by 11.1 mm long) milled into the outer surface of the coil. Epoxy cement was used to hold the thermocouples in place. Two-dimensional finite-difference models were solved for both types of thermocouple installation. In the models, the installations could be assigned effective thermal conductivities normal to and parallel with the wall, and heat transfer coefficients could be specified on both sides of the wall. For a wide range of parameter values, and for typical wall temperature drops measured in the experimental work, the models predicted that the thermocouple installations would not significantly distort the temperature field in the wall.

Experimental procedures

The apparatus required 3–4 h to reach steady-state, mainly due to thermal lag in the insulation on the straight pipes connected to the coil. When steady-state was reached, 10–12 scans were made through the 30 wall thermocouples using the data logger. Multiple readings for each thermocouple were later averaged for the data analysis. Data for a single random scan through the 30 thermocouples never differed drastically from the averaged data. An identical procedure was used for the second half of each run, after reversing the direction of the gas flow through the coil. The gas flow rate was very steady through an entire run.

ANALYSIS OF DATA

Temperatures exactly at the inside and outside surfaces of the coil were obtained by logarithmically extrapolating the measured temperatures just inside the surfaces. A logarithmic dependence is predicted analytically for a cylindrical geometry for 1-dim. conduction in the radial direction. Inspection of the interior wall temperatures resulting from numerical solution of equation (1) verified that logarithmic extrapolation was an excellent approximation even with significant peripheral conduction of heat in the wall. Cubic least-squares curve fits were then determined for the five temperatures at the outside surface and also for the five temperatures at the inside surface, for each of the six axial positions on the coil. A cubic fit provided some smoothing of the data and gave reasonable representations of the surface temperature profiles. Equation (1) was then solved at each of the six axial positions on the coil, and the peripherally averaged heat flux $\bar{q}$ at the inside surface of the coil at each position was evaluated using equations (2) and (5).

The gas heat duty was calculated from the flow rate and bulk temperatures at the coil inlet and outlet. An average heat flux for the coil, q_{avg}, was calculated from this duty and the coil inside surface area. If the data analysis is to be consistent, q_{avg} calculated in this manner must be the same as that obtained by integrating $\bar{q}$ along the coil. A trapezoidal-rule integration was found to be sufficiently accurate, yielding

$$q_{avg} = \frac{1}{7}\left(\frac{\bar{q}_0}{2} + \sum_{n=1}^{6} \bar{q}_n + \frac{\bar{q}_7}{2}\right). \tag{6}$$

Values of $\bar{q}_1$–$\bar{q}_6$ in this equation are the measured peripherally averaged heat fluxes at the six axial positions. The average heat flux exactly at the coil outlet, $\bar{q}_7$, was calculated by solving coupled equations for condensation outside the coil (using Nusselt's equation for condensation on a horizontal cylinder), conduction through the stainless steel wall, and convection inside the coil at that point. The gas convective heat transfer coefficient at the coil outlet was assumed equal to the average coefficient for the entire coil based on logarithmic-mean temperature difference. It is readily shown that, for the UWT condition, the average coefficient based on logarithmic-mean temperature difference becomes equal to the fully developed heat transfer coefficient when the tube is sufficiently long. The experimental results confirmed that this was a reasonable procedure for estimating $\bar{q}_7$. Calculated values of $\bar{q}_7$ always fell in line with a smooth extrapolation from the heat fluxes measured in the central region of the coil. The heat balance was closed by rearranging equation (6) in the form

$$\bar{q}_0 = 2\left(7q_{avg} - \sum_{n=1}^{6} \bar{q}_n - \frac{\bar{q}_7}{2}\right), \tag{7}$$

where $\bar{q}_0$ is a fictitious heat flux exactly at the coil inlet. The resulting flux distribution along the coil was then consistent with the gas temperatures at the coil inlet and outlet, and T_b at the various axial positions was calculated using trapezoidal-rule integration for the average heat flux between successive axial positions. Nusselt numbers were then calculated from equations (3) and (4).

Experimental investigation of the fully developed heat transfer region with the UWT condition poses an interesting, and difficult, problem: As investigation proceeds farther and farther into this region, $\bar{q}$ necessarily becomes more difficult to measure since it is decreasing to zero exponentially [29]. Therefore, any measurement technique, no matter how accurate, will eventually reach a point where error becomes intolerable. This point was reached in the present study in the vicinity of the last two axial positions on the coil. Near the coil outlet, T_b approached $\bar{T}_w$, and the resulting wall temperature drops approached the limit of accuracy of the temperature measurements. This resulted in unreliable values of $\bar{q}_6$ and, for some runs, $\bar{q}_5$. In these instances, the values of $\bar{q}_5$ and $\bar{q}_6$ used in equation (7) were obtained by interpolating visually between $\bar{q}_7$, which was rigorously calculated, and the heat fluxes measured in the central region of the coil.

An approximate independent check on the heat balance between the coil inlet ($x/d = 0$) and the first axial position ($x/d = 13.53$) indicated that the above heat balance procedures were reasonable. Reynolds *et al.* [30] developed an analytical solution for turbulent, straight-tube entrance-region flow of gases with the UHF boundary condition. The turbulent velocity profile was fully developed at the entrance. Their results were correlated to within ±5% by

$$Nu_s/Nu_{s,\infty} = 1 + 0.8\,(1 + 70\,000\,Re^{-3/2})\,(x/d)^{-1} \tag{8}$$

$$3000 \leqslant Re \leqslant 50\,000.$$

Their fully developed Nusselt numbers could be represented to within 4% by a Dittus–Boelter equation of the form

$$Nu_{s,\infty} = 0.021\,Re^{0.8}\,Pr^{0.4}. \tag{9}$$

For all Reynolds numbers, the fully developed Nusselt number was reached within 30 diameters. Deissler's [28] solutions for turbulent flow in straight tubes indicate that UHF and UWT Nusselt numbers agree to within about 10% over the entire thermal-entrance region. Accordingly, for runs which had turbulent flow at the coil inlet, equation (8) was used to estimate the heat transferred to the gas in the region $0 \leqslant x/d \leqslant 13.53$. For UWT conditions, neither the $\bar{q}$ nor the T_b distributions along the tube are known beforehand. These were calculated iteratively using equation (8).

The average heat flux in the region $0 \leqslant x/d \leqslant 13.53$ was calculated from the converged results and compared with $(\bar{q}_0 + \bar{q}_1)/2$, the corresponding average heat

flux obtained by forcing the heat balance. For the 12 runs with air, and compared to the latter average heat flux, the average heat flux calculated using equation (8) had an average deviation of -2.2% and a standard deviation of $\pm 10\%$. This relatively good agreement can be taken as an indication that the measured heat fluxes were reliable (except near the outlet as noted above) and that the method of forcing the heat balance was reasonable.

RESULTS AND DISCUSSION

Table 2 summarizes the experimental runs. Runs were not made with air for $Re < 2500$, because wall temperature drops were too small to be measured accurately. The single helium run was successful in extending measurements down to $Re = 1610$. For the present conditions, $k_{He} \cong 6k_{air}$. Therefore, reasonably high heat fluxes were obtained with helium, even though the Reynolds number was lower than those of the runs with air. Table 2 also lists Nu_{lm}, the average Nusselt number for the coil based on a logarithmic mean temperature difference. Nu_{lm} is defined by

$$Nu_{lm} = \frac{Re\,Pr}{4(L/d)} \ln\left(\frac{T_w - T_{b,in}}{T_w - T_{b,out}}\right) \qquad (10)$$

where the average temperature for the entire inside surface of the coil was used for T_w. Physical properties were based on the average gas bulk temperature.

All of the air runs had fully developed, straight-tube, turbulent velocity profiles at the coil inlet. If the Reynolds number is less than the curved-tube critical Reynolds number, the dye-injection experiments of Taylor [3] indicate that the turbulence will decay and be replaced by steady laminar flow. Srinivasan *et al.* [31] proposed the following correlation for curved-tube critical Reynolds number:

$$Re_c = 2100[1 + 12(a/R)^{1/2}]. \qquad (11)$$

Equation (11) gives $Re_c = 8600$ for the present coil. For Run 13 with $Re = 12\,800$, the air was very likely turbulent throughout the coil.

Table 2. Summary of experimental run conditions

Run	Gas	Re	De	Pr	Nu_{lm}
1	He	1610	416	0.67	15.2
2	air	2520	649	0.71	17.8
3	air	3300	851	0.71	24.1
4	air	3870	997	0.71	24.4
5	air	5230	1350	0.71	28.5
6	air	5240	1350	0.71	28.4
7	air	5260	1350	0.71	27.1
8	air	6930	1780	0.71	31.2
9	air	7840	2020	0.71	33.4
10	air	8360	2150	0.71	35.7
11	air	9200	2370	0.71	37.2
12	air	9240	2380	0.71	37.6
13	air	12800	3300	0.71	48.2

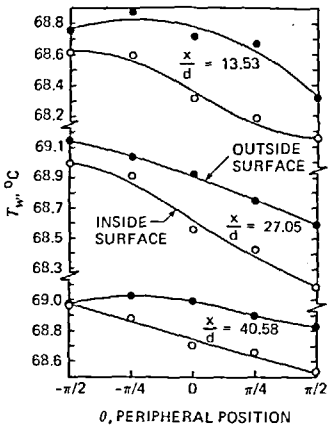

FIG. 2(a). Typical extrapolated surface temperatures and least-squares cubic curve fits at the first three axial positions on the coil (Run 9, $Re = 7840$).

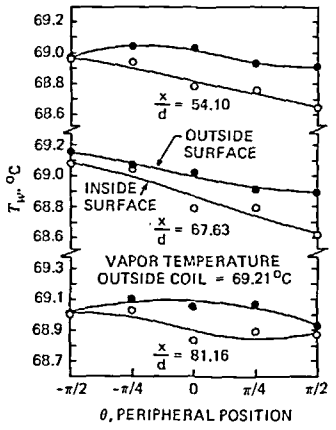

FIG. 2(b). Typical extrapolated surface temperatures and least-squares cubic curve fits at the last three axial positions on the coil (Run 9, $Re = 7840$).

Figures 2(a) and (b) show typical extrapolated surface temperatures with their least-squares cubic fits. For all of the runs, significant peripheral variation in the gas heat transfer coefficient was already in effect at $x/d = 13.53$, as evidenced by the skewing of the wall temperatures to lower values at the outside of the coil bend ($\theta = \pi/2$). By $x/d = 40.58$, the wall-temperature profiles have become approximately similar in shape, with nearly the same temperatures being measured at the inside and outside surfaces at the inside of the coil bend ($\theta = -\pi/2$). The resulting very small temperature drop across the wall at this location and the general shape of the temperature profiles indicate that the heat transfer coefficients at the inside of the bend are considerably smaller than those at the outside of the bend. For laminar-flow heat transfer to gases ($Pr = 0.7$), numerical solutions [15, 27] for the UWT condition indicate that Nu at the inside of the bend can be an order of magnitude or more smaller than Nu at the outside of the bend and can even fall below the straight-tube fully developed value, $Nu_{s,\infty} = 3.657$.

The low value of Nu at the inside of the bend is a consequence of the secondary flow, which circulates into this region fluid which has been heated close to the wall temperature.

In some instances, the cubic fits gave a slight temperature crossover (inside coil surface hotter than outside surface) at $\theta = -\pi/2$. These crossovers were always within the estimated uncertainty of the temperature drop across the wall ($\pm$ 0.04°C). No attempt was made to adjust the least-squares fits to eliminate these small crossovers, as this would have biased the results. When these small temperature crossovers occurred, small negative values of Nu were calculated at $\theta = -\pi/2$; however, this is not indicative of a real phenomenon. The peripherally averaged quantities $\bar{q}$ and $\overline{Nu}$, resulting from an integration procedure, are expected to be significantly more accurate than q and Nu, which were obtained by differentiation of the numerically calculated temperature field within the wall and which are sensitive to the type of curve fit chosen for the surface temperatures.

Figure 3 shows typical axial distributions of $\bar{q}$. Once this heat flux distribution is known, the gas bulk-temperature distribution can be calculated. Typical results are shown in Fig. 4. Values of $\bar{T}_w$ exactly at the coil inlet and outlet are calculated values; the remaining six points are measured values. Note that the experimental conditions are an excellent approximation to the UWT condition.

Experimental values of Nu_{lm} are compared in Fig. 5 with various correlations for the fully developed Nusselt number. Based on their numerical solution with the UWT condition, Kalb and Seader [15] correlated the fully developed peripherally averaged Nusselt number for $0.7 \leqslant Pr \leqslant 5$ with

$$\overline{Nu}_x = 0.836\, De^{1/2}\, Pr^{1/10},\ De \geqslant 80. \qquad (12)$$

For the present coil with $R/a = 15.06$, equation (12) applies for $310 \leqslant Re \leqslant Re_c$. If the datum point at $Re = 12\,800$ is omitted, the remaining 12 values of Nu_{lm} have an average deviation from equation (12) of only -5.9%. A deviation in this direction may be the result of insufficient coil length for Nu_{lm} to approach very close to the fully developed Nusselt number.

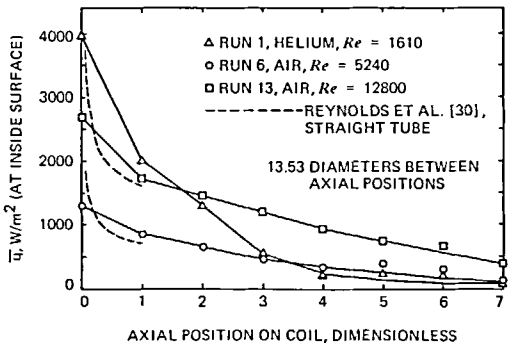

FIG. 3. Typical axial distribution of peripherally averaged heat flux.

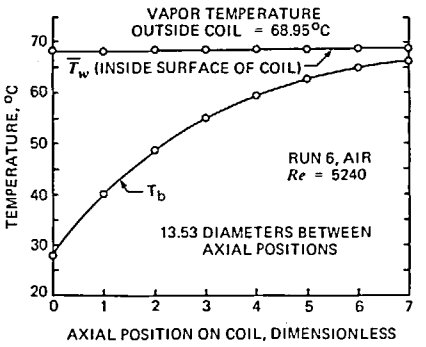

FIG. 4. Typical axial variation of gas bulk temperature and peripherally averaged wall temperature.

Using an approximate boundary layer analysis for the high Dean number laminar region, Mori and Nakayama [32] proposed the following equation for both UWT and UHF conditions:

$$\overline{Nu}_\infty = (0.864/\xi)\, De^{1/2}\,(1 + 2.35\, De^{-1/2}) \qquad (13)$$

where

$$\xi = \frac{1}{5}\left[2 + \left(\frac{10}{Pr^2} - 1\right)^{1/2}\right] \qquad (14)$$

when $Pr \leqslant 1$. Equation (13), shown in Fig. 5, is also in reasonable agreement with the experimental values of Nu_{lm}.

Correlations for the turbulent fully developed Nusselt number are also shown in Fig. 5. Mori and Nakayama's turbulent boundary layer analysis led to the following relation for gases with Prandtl number of order unity, for both UWT and UHF conditions:

$$\overline{Nu}_\infty = \frac{Pr\, Re^{4/5}\,(a/R)^{1/10}}{26.2\,(Pr^{2/3} - 0.074)} \times \left\{1 + \frac{0.098}{[Re\,(a/R)^2]^{1/5}}\right\},\ Re\,(a/R)^2 > 0.1. \qquad (15)$$

Rogers and Mayhew's [33] results are typical of

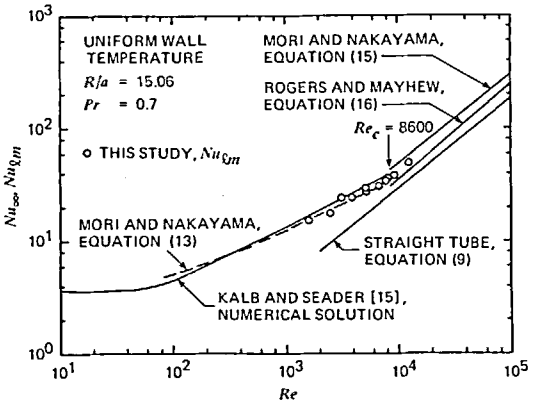

FIG. 5. Comparison of experimentally determined logarithmic-mean Nusselt number with correlations for fully developed Nusselt number.

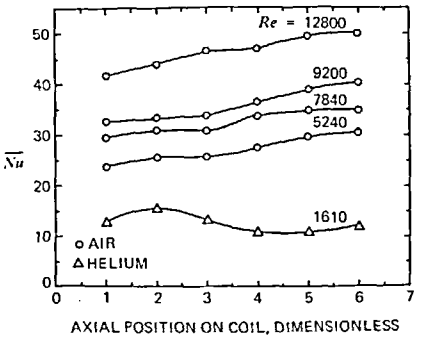

FIG. 6. Typical axial variation of peripherally averaged Nusselt number.

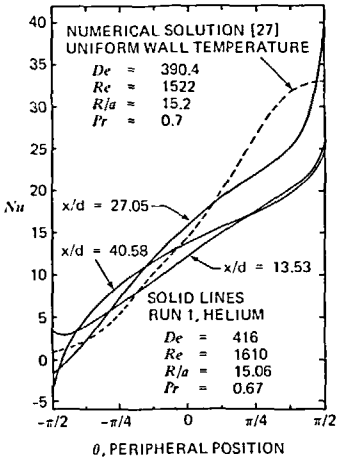

FIG. 7. Typical variation in Nu around the tube cross section and comparison with numerical solution.

various empirical correlations proposed for turbulent convection in curved tubes. Based on their data for water flowing through steam-heated coils, they proposed the relation

$$\overline{Nu}_x = 0.023\, Re^{0.85}\, Pr^{0.4}\,(a/R)^{0.1}. \qquad (16)$$

The present experimental data in the vicinity of Re_c fall between equations (15) and (16). For comparison, the straight-tube fully developed Nusselt number predicted by equation (9) is also shown in Fig. 5.

Several interesting observations may be made from Fig. 5. Note the relatively smooth transition between laminar and turbulent curved-tube Nusselt numbers. For R/a as small as 15.06, the curved-tube friction factor also undergoes a smooth transition in passing from laminar to turbulent flow. This is in contrast to straight-tube flow, where sharp discontinuities occur in both the Nusselt number and the friction factor with the onset of turbulence. Also note that, for given Re, Nu_x is higher for curved-tube laminar flow than for straight-tube turbulent flow. As a consequence, Nu_{lm} approaches Nu_x from below in the turbulent-to-laminar transition regime.

For the air runs of the present study, the gas entered the coil with a fully developed straight-tube turbulent velocity profile. For $Re \lesssim 8600$, fully developed laminar flow should have developed somewhere within the first turn of the coil. Therefore, local Nusselt numbers near the coil outlet are expected to be close to fully developed values, and transition must occur along the coil between straight-tube and curved-tube heat transfer behavior. Measured values of $\overline{Nu}$ shown in Fig. 6 confirm this picture, with $\overline{Nu}$ increasing in the flow direction and tending toward fully developed values. The trend shown in Fig. 6 for the helium run may be a real phenomenon, as oscillatory behavior in entrance-region Nusselt numbers has been noted for laminar flow in both theoretical [14, 16–18] and experimental [16, 18, 19] studies.

Experimentally determined local Nusselt numbers around the periphery of the tube cross section are compared in Fig. 7 with a numerical solution for fully developed heat transfer [15, 27]. Fig. 7 shows that, even at the first instrumented position on the coil (x/d = 13.53), a large spread had been established in Nu from inner to outer walls. The quantitative agreement with the numerical solution is encouraging, considering that the experimental results were derived from a relatively small number of temperature measurements made within a wall across which temperature differences were very small. The upward inflection of the experimental curves in the vicinity of the outer wall ($\theta = \pi/2$), along with the aforementioned small negative values of Nu at the inner wall ($\theta = -\pi/2$), are not real phenomena, but artifacts of the least-squares cubic curve fits used for the surface temperatures. Other curve fits involving, e.g. derivative conditions at $\theta = \pm \pi/2$, possibly could have eliminated these anomalies in some instances, but it was felt that the scatter in the raw data did not justify use of more-sophisticated techniques. It is expected that $\overline{Nu}$ would be insensitive to the nature of the curve fit chosen for the surface temperatures since $\overline{Nu}$ is derived by an integrating, or averaging, procedure. Values of Nu, however, being derived from differentiation of the calculated temperature field within the wall, are quite sensitive to the type of curve fit used. Despite this problem, Fig. 7 can be taken as direct experimental confirmation of the large peripheral variation which exists in local heat transfer coefficients for laminar flow in curved tubes.

No relevant criteria are available for evaluating the possible influence of free-convection effects in a helical coil with horizontal axis. However, conservative comparison (Grashof number based on the inlet temperature difference) with straight-tube criteria [34] indicates that the present experimental conditions were well within the region where forced convection dominates.

SUMMARY AND CONCLUSIONS

A gradient method was developed for measuring entrance-region heat transfer coefficients in a uniform wall-temperature helical coil. The coefficients mea-

sured in a two-turn coil varied both longitudinally and circumferentially. Measurements included the regime where the flow is initially turbulent upon entering the coil, but laminar downstream where secondary flow develops. For heat transfer to gases in this regime, the local peripherally averaged Nusselt number increased along the coil and approached close to fully developed values near the coil outlet. For gases flowing in helical coils of two or more turns, the fully developed Nusselt number can be used with little error for design or rating of the entire coil.

Acknowledgement—This research was supported primarily through a NASA Traineeship in the Chemical Engineering Department at the University of Utah.

REFERENCES

1. R. L. Manlapaz and S. W. Churchill, Fully developed laminar flow in a helically coiled tube of finite pitch, *Chem. Engng Commun.* **7**, 57–78 (1980).
2. C. M. White, Stream-line flow through curved pipes, *Proc. R. Soc.* **A123**, 645–663 (1929).
3. G. I. Taylor, The criterion for turbulence in curved pipes, *Proc. R. Soc.* **A124**, 243–249 (1929).
4. L. R. Austin and J. D. Seader, Entry region for steady viscous flow in coiled circular pipes, *A.I.Ch.E. Jl* **20**, 820–822 (1974).
5. S. V. Patankar, V. S. Pratap and D. B. Spalding, Prediction of laminar flow and heat transfer in helically coiled pipes, *J. Fluid Mech.* **62**, 539–551 (1974).
6. M. Rowe, Measurements and computations of flow in pipe bends, *J. Fluid Mech.* **43**, 771–783 (1970).
7. Y. Agrawal, L. Talbot and K. Gong, Laser anemometer study of flow development in curved circular pipes, *J. Fluid Mech.* **85**, 497–518 (1978).
8. L. S. Yao and S. A. Berger, Entry flow in a curved pipe, *J. Fluid Mech.* **67**, 177–196 (1975).
9. J. A. C. Humphrey, Numerical calculation of developing laminar flow in pipes of arbitrary curvature radius, *Can. J. Chem. Engng* **56**, 151–164 (1978).
10. M. Akiyama and K. C. Cheng, Boundary vorticity method for laminar forced convection heat transfer in curved pipes, *Int. J. Heat Mass Transfer* **14**, 1659–1675 (1971).
11. C. E. Kalb and J. D. Seader, Heat and mass transfer phenomena for viscous flow in curved circular tubes, *Int. J. Heat Mass Transfer* **15**, 801–817 (1972).; also errata, *Int. J. Heat Mass Transfer* **15**, 2680 (1972).
12. N. J. Rabadi, J. C. F. Chow and H. A. Simon, An efficient numerical procedure for the solution of laminar flow and heat transfer in coiled tubes, *Num. Heat Transfer* **2**, 279–289 (1979).
13. M. Akiyama and K. C. Cheng, Laminar forced convection heat transfer in curved pipes with uniform wall temperature, *Int. J. Heat Mass Transfer* **15**, 1426–1431 (1972).
14. J. M. Tarbell and M. R. Samuels, Momentum and heat transfer in helical coils, *Chem. Engng Jl* **5**, 117–127 (1973).
15. C. E. Kalb and J. D. Seader, Fully developed viscous-flow heat transfer in curved circular tubes with uniform wall temperature, *A.I.Ch.E. Jl* **20**, 340–346 (1974).
16. A. N. Dravid, K. A. Smith, E. W. Merrill and P. L. T. Brian, Effect of secondary fluid motion on laminar flow heat transfer in helically coiled tubes, *A.I.Ch.E. Jl* **17**, 1114–1122 (1971).
17. M. Akiyama and K. C. Cheng, Laminar forced convection in the thermal entrance region of curved pipes with uniform wall temperature, *Can. J. Chem. Engng* **52**, 234–240 (1974).
18. L. A. M. Janssen and C. J. Hoogendoorn, Laminar convective heat transfer in helical coiled tubes, *Int. J. Heat Mass Transfer* **21**, 1197–1206 (1978).
19. R. A. Seban and E. F. McLaughlin, Heat transfer in tube coils with laminar and turbulent flow, *Int. J. Heat Mass Transfer* **6**, 387–395 (1963).
20. *Thermophysical Properties Research Center Data Book*, Vols 1 and 2. Purdue University, Lafayette, Indiana (1964).
21. V. K. Shchukin and A. F. Koval'nogov, The use of computers in the gradient method of heat transfer, *Soviet Aeronaut.* **10**, 74–79 (1967).
22. V. K. Shchukin and A. A. Khalatov, Generalization of the gradient heat-transfer analysis method to the case of arbitrary temperature dependence of the wall material thermal conductivity, *Soviet Aeronaut.* **12**, 81–84 (1969).
23. V. K. Shchukin, A. A. Khalatov and V. A. Filin, The gradient method for the study of heat transfer in variable cross section channels, *Heat Transfer, Soviet Res.* **2**, 157–163 (1970).
24. V. I. Goldobeev, V. K. Shchukin, A. A. Khalatov and A. P. Yakshin, Heat transfer in initial segment of pipe with partial swirl of gas stream at the entrance, *Soviet Aeronaut.* **16**, 81–85 (1973).
25. V. K. Shchukin and V. V. Olimpiev, Heat transfer between rotating disks in a closed cavity, *J. Engng Phys.* **30**, 394–399 (1976).
26. N. N. Koval'nogov, Application of gradient method to study of heat transfer in axisymmetric channels of different configuration, *Soviet Aeronaut.* **22**, 80–83 (1979).
27. C. E. Kalb, Viscous-flow heat transfer in curved tubes, Ph.D. dissertation, University of Utah, Salt Lake City (1973).
28. R. G. Deissler, Analysis of turbulent heat transfer and flow in the entrance regions of smooth passages, National Advisory Committee for Aeronautics, Technical Note 3016 (1953).
29. S. Hasegawa and Y. Fujita, Turbulent heat transfer in a tube with prescribed heat flux, *Int. J. Heat Mass Transfer* **11**, 943–962 (1968).
30. H. C. Reynolds, T. B. Swearingen and D. M. McEligot, Thermal entry for low Reynolds number turbulent flow, *J. Basic Engng* **91**, 87–94 (1969).
31. P. S. Srinivasan, S. S. Nandapurkar and F. A. Holland, Pressure drop and heat transfer in coils, *Chem. Engr* No. 218, 113–119 (1968).
32. Y. Mori and W. Nakayama, Study on forced convective heat transfer in curved pipes (3rd report, theoretical analysis under the condition of uniform wall temperature and practical formulae), *Int. J. Heat Mass Transfer* **10**, 681–695 (1967).
33. G. F. C. Rogers and Y. R. Mayhew, Heat transfer and pressure loss in helically coiled tubes with turbulent flow, *Int. J. Heat Mass Transfer* **7**, 1207–1216 (1964).
34. B. Metais and E. R. G. Eckert, Forced, mixed and free convection regimes, *Trans. Am. Soc. Mech. Engrs.* Series C, *J. Heat Transfer* **86**, 295–296 (1964).

TRANSFERT THERMIQUE DANS LA REGION D'ENTREE D'UN SERPENTIN A TEMPERATURE UNIFORME EN PAROI AVEC TRANSITION DU TURBULENT AU LAMINAIRE

Résumé—On étudie expérimentalement le transfert thermique dans la région d'entree d'un serpentin à température pariétale uniforme. Une nouvelle méthode de gradient est basée sur la mesure des distributions de température sur les surfaces interne et externe. Les mesures sont faites dans le domaine des nombres de Reynolds où l'écoulement est initialement turbulent à l'entrée du serpentin mais devient laminaire en aval quand se développe l'écoulement secondaire. Aucune mesure n'a été décrite jusqu'ici pour les coefficients locaux de transfert thermique dans ce régime d'écoulement ou cette condition aux limites. Les résultats montrent une transition rapide vers l'écoulement laminaire et un accord satisfaisant est constaté avec la solution numérique pour le transfert thermique pleinement établi.

DER WÄRMEÜBERGANG IM EINTRITTSBEREICH EINER ROHRSPIRALE MIT KONSTANTER WANDTEMPERATUR MIT ÜBERGANG VON TURBULENTER ZU LAMINARER STRÖMUNG

Zusammenfassung—Der Wärmeübergang an Gase wurde im Eintrittsbereich einer Rohrspirale mit konstanter Wandtemperatur experimentell untersucht. Ein neuartiges Gradientenverfahren für die Untersuchung von Wärmeübergangsproblemen wurde entwickelt, das auf der Messung der Temperaturverteilung an der Innen- und Außenseite beruht. Die Versuche wurden in einem Bereich der *Re*-Zahl durchgeführt, in dem die Strömung am Eintritt in die Spirale turbulent ist und weiter stromab infolge von Sekundärströmungen laminar wird. Es gibt keine früheren Messungen der örtlichen Wärmeübergangskoeffizienten für diesen Strömungszustand und diese thermische Randbedingung. Die Ergebnisse zeigen einen schnellen Übergang zu laminarer Strömung und befriedigende Übereinstimmung mit einer numerischen Lösung für vollständig ausgebildeten Wärmeübergang.

ТЕПЛОПЕРЕНОС ВО ВХОДНОЙ ОБЛАСТИ СПИРАЛЬНОГО ЗМЕЕВИКА С ОДНОРОДНОЙ ТЕМПЕРАТУРОЙ СТЕНОК ПРИ ПЕРЕХОДЕ РЕЖИМА ТЕЧЕНИЯ ОТ ТУРБУЛЕНТНОГО К ЛАМИНАРНОМУ

Аннотация—Экспериментально исследован теплоперенос во входной области при течении газов в спиральном змеевике с однородной температурой стенок. Разработан новый градиентный метод исследования теплопереноса, основанный на измерении распределения температур на внутренней и внешней поверхностях стенок. Эксперименты проводились в диапазоне значений числа Рейнольдса, при которых вначале (на входе в змеевик) поток является турбулентным, а затем переходит в ламинарный в области вниз по течению, где развивается вторичное течение. Данные по коэффициентам локального теплообмена для такого типа течения и тепловых граничных условий ранее не публиковались. Полученные результаты указывают на быстрый переход к ламинарному режиму и удовлетворительно согласуются с численным решением для полностью развитого процесса теплопереноса.